Noise in solid-state nanopores

R. M. M. Smeets*, U. F. Keyser*†, N. H. Dekker*, and C. Dekker*‡

*Kavli Institute of Nanoscience, Delft University of Technology, Lorentzweg 1, 2628 CJ Delft, The Netherlands; and †Institut fur Experimentelle Physik 1, Universität Leipzig, Linnéstrasse 5, 04103 Leipzig, Germany

Edited by Robert H. Austin, Princeton University, Princeton, NJ, and approved November 13, 2007 (received for review June 7, 2007)

We study ionic current fluctuations in solid-state nanopores over a wide frequency range and present a complete description of the noise characteristics. At low frequencies ($f \lesssim 100$ Hz) we observe 1/*f*-type of noise. We analyze this low-frequency noise at different salt concentrations and find that the noise power remarkably scales linearly with the inverse number of charge carriers, in agreement with Hooge's relation. We find a Hooge parameter $\alpha = (1.1 \pm 0.1) \times 10^{-4}$. In the high-frequency regime ($f \gtrsim 1$ kHz), we can model the increase in current power spectral density with frequency through a calculation of the Johnson noise. Finally, we use these results to compute the signal-to-noise ratio for DNA translocation for different salt concentrations and nanopore diameters, yielding the parameters for optimal detection efficiency.

Nanometer-sized pores can be used as versatile sensors for single biomolecules such as DNA, RNA, or proteins. The charged molecules are electrophoretically driven through the nanopore, resulting in temporal changes of the ionic current. The technique was first demonstrated by measuring the passage of DNA and RNA through the protein pore α-hemolysin (1). More recently, solid-state nanopores were developed and used to measure the traversal of polynucleotides (2). These translocation experiments have already addressed a wide range of interesting properties of nucleic acids (3). Fabricated solid-state nanopores have obvious advantages over their biological counterparts, such as high stability, adjustable geometry, and surface properties, and the potential of integration into devices. However, to date, they have been accompanied by a large variability in low-frequency noise, which limits their sensitivity and reliability (4, 5). Studies of the ionic current noise can provide detailed information on dynamic processes occuring in the nanoscale volume of a single nanopore, and can help to improve and optimize nanopore characteristics. In protein pores, the protonation of ionization sites (6), the transport of sugars (7–10), ATP (11), and antibiotic molecules (12), and the conformational dynamics of protein pores (13) were all detected by studying ionic current fluctuations. On fabricated nanopores, only a few noise studies were performed so far, which related an increased low-frequency noise to the motion of polymeric subunits constituting the channel walls (14), and to the presence of nanometer-sized bubbles (nanobubbles) inside the nanopore (5).

In this article, we present a complete picture of the current noise of fabricated solid-state nanopores by addressing both the low- and high-frequency regimes. We first give a brief overview of the general characteristics of our nanopores, showing a linear current–voltage (I–V) relation with resistance values that can vary significantly from pore-to-pore. We compare current-time traces and power spectra of illustrative nanopores of similar diameter but substantially different resistance, and we find that, whereas the high-frequency noise is of comparable magnitude, the low-frequency 1/*f* noise can be dramatically different. We show that the high-frequency current power spectral density is well described by the Johnson noise in our electrical circuit. Subsequently, we study the low-frequency 1/*f* noise in nanopores with resistance values that fit the nanopore geometry, and we identify that this noise can be related to the number of charge carriers, as described by the Hooge relation. We conclude by using our results in a calculation of the signal-to-noise ratio of DNA translocation through these solid-state nanopores. Surprisingly, we find that large nanopores ($d_{pore} > 20$ nm) have improved signal-to-noise ratios in low-salt compared to high-salt regimes.

Results

General Nanopore Characteristics. Fig. 1*a* shows an example of I–V measurements at 1 M KCl of six individual nanopores with different diameters (Fig. 1*a Inset* shows a transmission electron micrograph of a 15.6 nm diameter pore). In all experiments, the I–V curves display a linear relationship. Linear fits to the data yield the value of the nanopore resistance, and the resistance of 28 individual nanopores as a function of diameter is plotted in Fig. 1*b*. As the nanopore diameter is increased from 3.7 to 51.0 nm, the resistance decreases from 480 to 3.5 MΩ. The measured resistance values show significant pore-to-pore variations, which we interpret as increases of the nanopore resistance from the resistance values expected by geometry. The red solid line shows the expected resistance of a 25-nm-long cylinder that scales as $1/d_{pore}^2$, where d_{pore} is the nanopore diameter (15). Although it coincides with some data points, many nanopores also exhibit a higher resistance. Nanopores with a large resistance value compared to the resistance of the cylinder ($\geq 2.5\times$) are shown in gray.

Fig. 1*c* shows current traces and histograms of two representative nanopores of similar ($\approx$21 nm) diameter, which differ substantially in resistance. Their resistance values can be deduced from the differing currents as 9.1 and 34.7 MΩ, where the higher resistance value is large compared to the expected resistance of 4.7 MΩ for a 25-nm-long cylinder. Both traces are recorded at an applied voltage of 100 mV and low-pass filtered at 10, and 1 kHz, as indicated. The 10-kHz filtered current traces (black and grey data in Fig. 1*c*) show strong differences in current noise, which is reflected in the width of their current histograms. The standard deviation of the current is 22.6 and 78.6 pA, for the black and grey traces, respectively. These differences become even more evident for the traces filtered at 1 kHz (red and blue data in Fig. 1*c*). From a comparison of the black and red current traces, it is apparent that the current noise is greatly reduced upon additional filtering. However, the 1-kHz filtered blue trace displays hardly any reduction of the large current fluctuations and width of the current histogram compared to the 10-kHz filtered grey trace. Indeed, upon filtering, the standard deviation of the current at 1 kHz decreases to 3.6 and 70.6 pA for the red and blue traces, respectively. We conclude that the current fluctuations of the nanopore with the large resistance (bottom traces) can be attributed to excessive low-frequency noise, as is also evident from the current power spectral densities shown in Fig. 1*d*. At frequencies below 200 Hz, both traces display 1/*f*-type of noise, which differs by nearly 3 orders of magnitude. The black

Author contributions: U.F.K., N.H.D., and C.D. designed research; R.M.M.S. and U.F.K. performed research; R.M.M.S. analyzed data; and R.M.M.S. wrote the paper.

The authors declare no conflict of interest.

This article is a PNAS Direct Submission.

‡To whom correspondence should be addressed. E-mail: c.dekker@tudelft.nl.

This article contains supporting information online at www.pnas.org/cgi/content/full/0705349105/DC1.

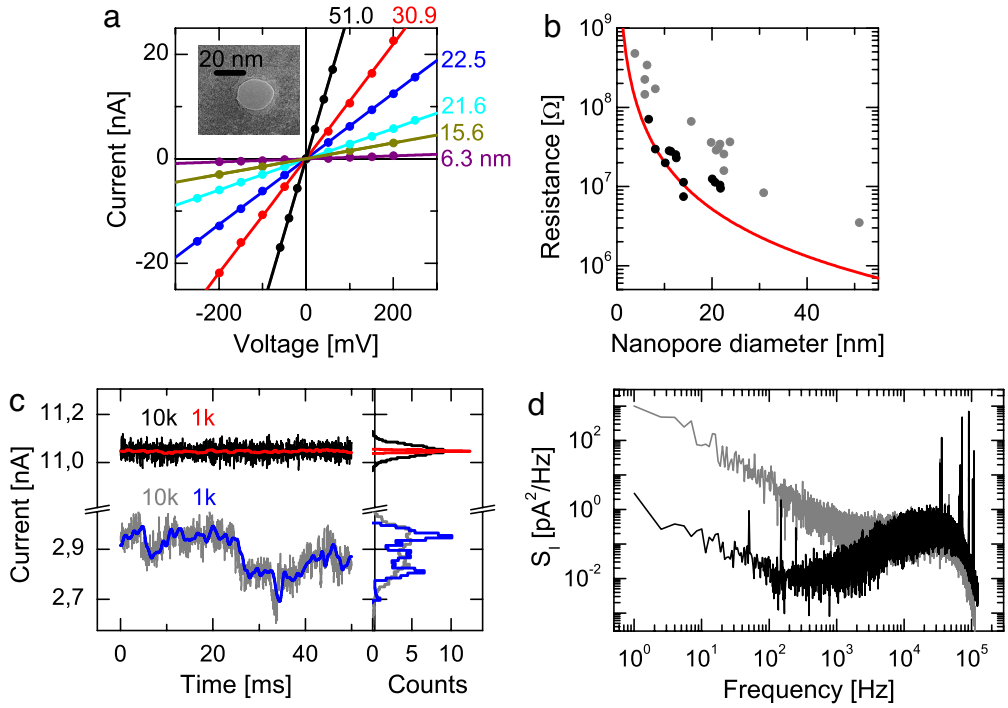

Fig. 1. General nanopore characteristics at 1 M salt. (*a*) Current–voltage characteristics of six individual nanopores with nanopore diameters as indicated. All curves show a linear I–V dependence. (*Inset*) A transmission electron microscopy image of the 15.6-nm-diameter nanopore. (*b*) Resistance values of 28 individual nanopores as a function of nanopore diameter. The red line represents the resistance of a 25-nm-long cylinder. Resistance values larger than 2.5 times the resistance indicated by the red line are shown in grey. (*c*) Current recordings and histograms of two nanopores (at 100 mV) with substantially different resistance values, illustrating clear differences in current noise. The nanopores diameters are 20.8 nm (bottom traces) and 22.0 nm (top traces). The current was filtered at 10 and 1 kHz, as indicated. The black, grey, and blue histograms, shown on the right, are magnified along the *x* axis to be visible on the same scale. (*d*) Current power spectral densities of the two nanopores used in *c*, showing 1/*f* low-frequency noise of different magnitude and comparable high-frequency noise.

trace displays 1/*f* noise up to ≈200 Hz, followed by an increase in current power spectral density up to ≈15 kHz, and ending with a relative flat region before filter attenuation. For the grey trace, 1/*f* noise dominates the current power spectral density up to frequencies of ≈2 kHz. At higher frequencies, the power spectrum appears flat until its attenuation by the low-pass frequency filter. Notice that, although the measured low-frequency noise is very different, the high-frequency noise of the nanopores in Fig. 1*d* is quite comparable.

The differences in low-frequency 1/*f* noise dramatically affect the current-time characteristics of these nanopores. In general, the magnitude of the 1/*f* noise shows strong pore-to-pore variations, with excessive low-frequency noise for nanopores with relatively high resistance values (grey data points in Fig. 1*b*). Here, we study the low-frequency noise for nanopores with resistances close to the values as expected from the nanopore geometry. For completeness, the low-frequency noise data of all nanopores is presented in the supporting information (SI) *Text* and SI Figs. 5–9.

Modeling the High-Frequency Current Noise. We model the high-frequency current power spectral density in our nanopore setup by a calculation of the Johnson noise (16). For details on the calculations and fits performed in this section, see *SI Text*. Taking the amplifier configuration into account, the current power spectral density can be calculated from the nanopore admittance Y_s (17). The nanopore is equivalent to a resistor R_p, in parallel with a capacitor C_p resulting from the liquid contact to the silicon chip containing the nanopore. We account for the nonideal behavior of this capacitor by inclusion of an admittance $Y = \omega C_p D$ in parallel with C_p, with D denoting the dielectric loss constant. The circuit is in series with a resistor R_c that represents the (relatively small) resistance from the electrodes to the nanopore. To determine Y_s, we apply a voltage step to our nanopore sample and measure the current response. Fig. 2*a* shows the current of a 15.6-nm-diameter nanopore before ($t < 0$) and after ($t \geq 0$) a 4-mV voltage step. We first assume $D = 0$ and extract the values of C_p and R_c by fitting the expected current response to the data, as shown by the red line in Fig. 2*a*. We obtain $C_p = 368 \pm 7$ pF and $R_c = 54.4 \pm 0.1$ kΩ. These values correspond to independently determined values of C_p on membranes that do not contain nanopores, and values of R_c measured without a nanopore sample present. The resistance R_p is obtained from a dc current-voltage measurement, such as shown in Fig. 1*a*, yielding $R_p = 67 \pm 2$ MΩ for the nanopore used. The value of the dielectric loss constant can now be determined from a closer inspection of the current response at long time scales. Fig. 2*b* shows the current response to the applied voltage step from $t = 0$ to $t = 10^4$ μs on a logarithmic scale. After an initial decrease, the current does not attain a steady-state value but continues to decrease up to 10^4 μs (equivalent to 500 R_cC_p). A fit of an ideal capacitor's response to the data is shown by the red line, which clearly fails to give a valid description for $t > 50$ μs. Alternatively, the current response at long time scales ($t > 40\ R_cC_p$) can be well described by Curie's law, which allows for a determination of the dielectric loss constant D (18). The blue line of Fig. 2*b* shows the best fit to the data for $t > 40R_cC_p$. We obtain $D = 0.27 \pm 0.07$, strongly deviating from $D = 0$ of an ideal capacitor.[§]

[§]The nonideal capacitor, C_p, can also be described only in terms of the model constants n and h as obtained from the best fit to Curie's law. The current power spectral density resulting from the use of these values is comparable to the calculated spectrum shown in Fig. 2*c*.

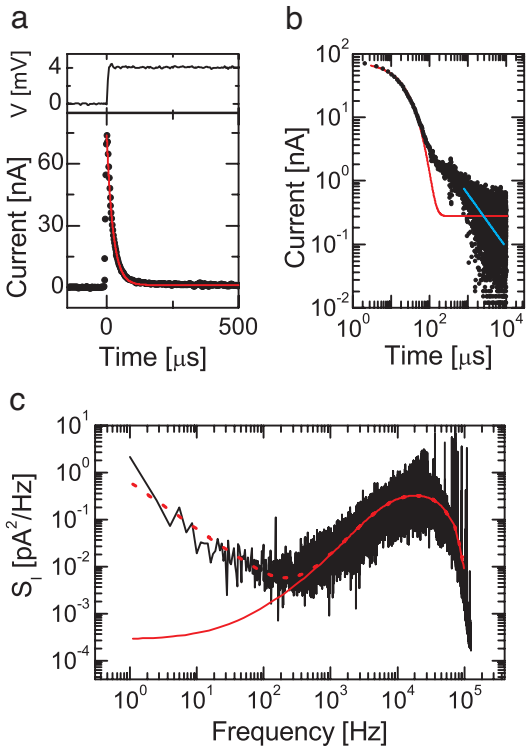

Fig. 2. Modeling the high-frequency current noise in nanopores. (*a*) The applied voltage and the resulting current response as a function of time for a 15.6-nm-diameter nanopore. The red line shows the best fit to the data. (*b*) The current response of *a* plotted on logarithmic scales for times up to 10^4 μs. The red line is identical to the one plotted in *a*, whereas the cyan line is a fit to Curie's law for $t > 40R_cC_p$. (*c*) Current power spectral density of a 15.6-nm-diameter nanopore (black) and the calculated power spectrum (red solid line). The red dotted line results from an addition of the measured low-frequency noise to the calculated values.

Having determined the values of all components of the nanopore admittance Y_s, we can now calculate the current power spectral density and compare it to the measured values. Fig. 2*c* shows the spectral density of the 15.6-nm-diameter nanopore in black. The calculated power spectral density is shown by the red solid line. For comparison, the effect of the filter used is taken into account. The modeled current power spectral density is flat at low frequencies, corresponding to the Johnson noise of the resistor $R_p + R_c \approx R_p$, followed by an increase due to the capacitance C_p, and finally reaching again a constant value, given by the Johnson noise of the resistor R_c alone. For high-frequency values (>20 kHz), the calculated spectrum decreases due to the filter cutoff. The model of the current power spectral density gives a good description of the data at frequencies >300 Hz. For lower frequencies, the measured power spectrum cannot be modeled, because it is not possible to *a priori* calculate the 1/*f* noise. Addition of the measured low-frequency noise to the calculated power spectrum yields the red dotted line of Fig. 2*c*, resulting in an excellent description of the data over the whole frequency range.

Low-Frequency 1/*f* Noise in Nanopores. We now turn to analyze the low-frequency 1/*f* noise in our solid-state nanopores. The nanopores analyzed have resistance values close to those expected from geometry. According to Hooge's phenomenological relation for low-frequency 1/*f* noise, the noise power, *A*, should scale inversely with the number of charge carriers N_c (19):

$$\frac{S_I}{I^2} = \frac{A}{f} = \frac{\alpha}{N_c f}, \qquad [1]$$

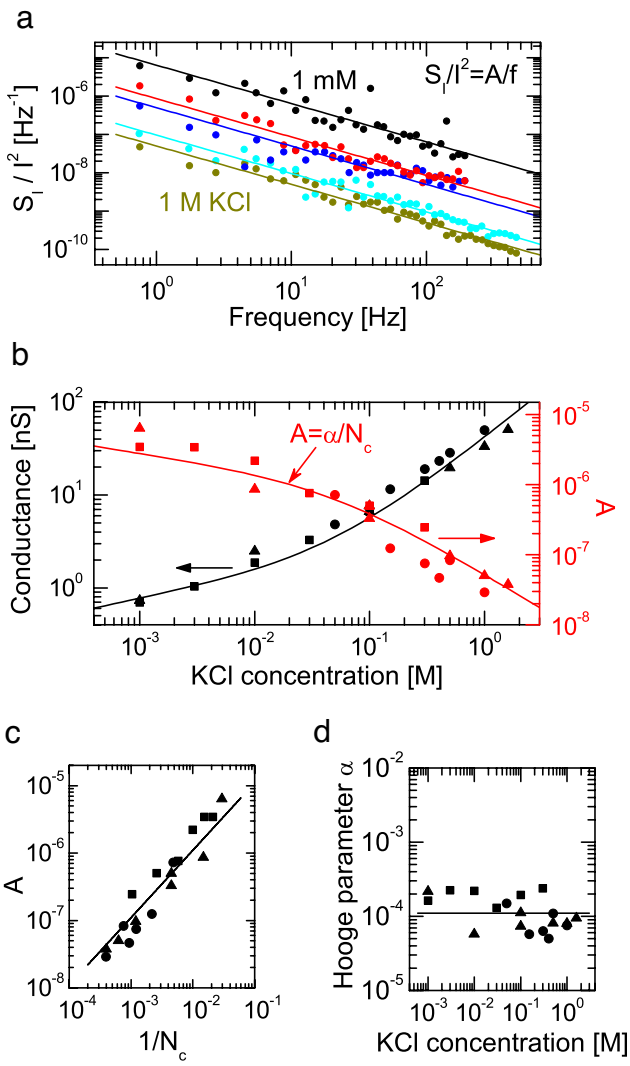

Fig. 3. Analysis of low-frequency 1/*f* noise in nanopores at different salt concentrations. (*a*) The normalized current power spectral density of an individual nanopore at salt concentrations of 1 mM (black), 10 mM (red), 100 mM (blue), 500 mM (cyan), and 1 M (yellow). The solid lines result from a fit of the data at each salt concentration to the formula shown. (*b*) Conductance and noise power of three nanopores from salt concentrations of 1 mM up to 1 M. Each individual nanopore has its own symbol. The black line shows the conductance of a cylindrical nanopore with an average nanopore diameter of d_{pore} = 9.3 nm, and a salt-dependent surface charge as given in ref. 15. The red line shows the noise power in terms of the number of charge carriers using $\alpha = 1.1 \times 10^{-4}$. (*c*) Noise power as a function of the calculated inverse number of charge carriers of the data shown in *b*. The black line indicates the linear scaling. (*d*) The value of the Hooge parameter over the salt concentration probed for the data shown in *b*. The Hooge parameter results from the product of the noise power and the number of charge carriers. The black line shows the constant value $\alpha = 1.1 \times 10^{-4}$.

where S_I is the current power spectral density, I is the current, f is the frequency, and α denotes the Hooge parameter, which quantifies the amount of low-frequency noise.[¶] We tested this relation by measuring the low-frequency noise of individual nanopores at different salt concentrations, because this is a means of varying N_c.

Fig. 3*a* shows the normalized current power spectral density

[¶]Alternatively, Hooge's equation can be presented as $S_I/I^2 = \alpha/N_c f^\beta$. Using this equation yields $0.7 < \beta < 1.4$ and essentially the same results as presented.

S_I/I^2 at low frequencies of a single nanopore at five different salt concentrations. All traces show 1/*f*-type of noise behavior, with variations up to 2 orders of magnitude. The data were fitted, using $S_I/I^2 = A/f$, as shown by the solid lines in Fig. 3*a*. As the salt concentration is increased, the value of the noise power decreases, with values of A ranging from 6.4×10^{-6} to 5.0×10^{-8}. Fig. 3*b* shows the conductance and noise power of three individual nanopores measured at salt concentrations from 1 mM up to 1 M. We observe that the conductance strongly increases as the salt concentration is increased (black points in Fig. 3*b*), but that the noise power shows a strong decrease (red points in Fig. 3*b*). The conductance does not show a linear dependence on potassium chloride concentration, due to the salt-dependent surface charge of the nanopore (15).

We now model the conductance in our nanopores to obtain a value for the number of charge carriers N_c and subsequently use this value to validate the use of Eq. **1**. The black line in Fig. 3*b* shows the conductance assuming a cylindrical nanopore geometry and the salt-dependent surface charge as given in ref. 15, which gives a good description of the data. From this we extract the number of ions in our nanopores N_c at each salt concentration. The red solid line now shows the best fit of the noise power $A = \alpha/N_c$ to the data, using Eq. **1** with one fitting parameter (α) only. We find a value of $\alpha = (1.1 \pm 0.1) \times 10^{-4}$, close to typical values found for electronic devices (20). The model describes the variation in noise power over the whole salt range remarkably well. Fig. 3 *c* and *d* shows different representations of the same data. Fig. 3*c* presents the noise power as a function of the calculated inverse number of charge carriers, showing the linear scaling (black line), in accordance with Hooge's relation. Fig. 3*d* shows the product of the noise power and the number of charge carriers, yielding a constant value of the Hooge parameter over the entire salt concentration probed. In conclusion, a variation of the noise power A in terms of a variation in the number of charge carriers N_c, gives an excellent description of the data.

Signal-to-Noise Ratio for DNA Translocation. Having fully characterized the current noise in the low- and high-frequency regime, we now turn to the signal-to-noise ratio (*SNR*) for DNA translocation. The *SNR* is calculated as a function of salt concentration, yielding an optimal range for DNA translocation experiments. The *SNR* is defined as

$$SNR = \frac{|\Delta I|}{I_{noise,RMS}}, \qquad [2]$$

where $I_{noise,RMS}$ is the root-mean-square current noise, and $|\Delta I|$ is the absolute current change due to DNA translocation. Note that $I_{noise,RMS}$ equals the square root of the integral of the low- and high-frequency current power spectral densities, $I_{noise,RMS} = (\int_0^{BW} S_I df)^{1/2}$, where BW is the bandwidth. Here we will consider low-frequency 1/*f*-type of noise with $\alpha = (1.1 \pm 0.1) \times 10^{-4}$, as determined above. The current power spectral density S_I at each salt concentration can then be calculated by using Eq. **1.** The high-frequency current power spectral density follows from a calculation of the Johnson noise, with the value of Y_s depending on the salt concentration. The DNA induced current change ΔI was experimentally measured before (15), and found to be linearly proportional to the salt concentration, with DNA translocation resulting in either decreases ($[KCl] > 0.4$ M) or increases ($[KCl] < 0.4$ M) of the ionic current. We assume the current change to be fully detectable at the used bandwidth of 10 kHz, which is valid for long (≳5 kbp) DNA molecules (for *SNR* calculations at 100 kHz, see *SI Text*). Possible effects at very low salt concentrations, such as Debye layer overlap and changes in the number of condensed counter-ions have not been considered.

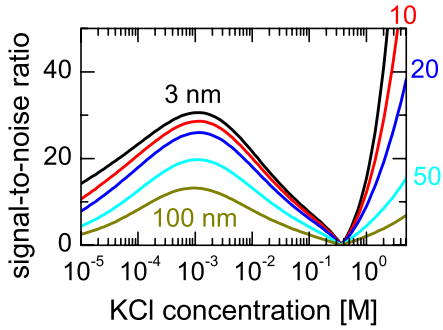

Fig. 4. SNR calculated for DNA translocation through five nanopores with different diameters as a function of salt concentration. The nanopore diameters are indicated. The smaller the nanopore, the better the SNR. For large nanopores ($d_{pore} > 20$ nm) measurements performed at low salt concentrations yield the best SNR.

Fig. 4 shows the resulting *SNR* as a function of salt concentration for five different nanopore diameters. When the salt concentration is lowered, the *SNR* initially decreases down to zero, because $|\Delta I| = 0$ when $[KCl] \approx 0.4$ M, and increases again reaching a local maximum at $[KCl] \approx 1 \times 10^{-3}$ M. At even lower salt concentrations the signal-to-noise ratio decreases again because the series resistance (R_c) becomes equal to or larger than the pore resistance (R_p), which results in a lower voltage drop over the nanopore. We have used $R_c = 200$ kΩ/$[KCl]$, but the same trend is observed for different values of R_c. Nanopores with smaller diameters have a better SNR for DNA translocation at all salt concentrations, as expected. At the commonly used potassium chloride concentration of 1 M, the SNR increases from 2 to 15 when the nanopore diameter is decreased from 100 to 3 nm. Higher values (≈50) are attainable at even higher salt concentrations. Surprisingly, we find that large nanopores ($d_{pore} > 20$ nm) have a better SNR in the low-salt compared to the high-salt regime. Detection of a single DNA molecule is even possible inside a nanopore with a diameter of $d_{pore} = 100$ nm, provided one measures at low salt concentrations.

Discussion and Conclusions

We have investigated the ionic current noise in our fabricated solid-state nanopores. The high-frequency noise can successfully be modeled by a calculation of the Johnson noise using a simple electrical circuit representation. The capacitance, which stems from the liquid contact to the silicon chip containing the nanopore, and the relative small resistance from the electrodes to the nanopore determine the current noise in the high-frequency regime. In the low-frequency regime, we measure a 1/*f*-type of noise behavior, which reflects the properties of our nanopores.

This noise power is found to vary from pore to pore, which results in dramatic differences in current-time characteristics. Nanopores with relatively high resistance values show excessive low-frequency 1/*f*-noise. This agrees well with the previously proposed presence of nanobubbles, which can account for the observed low-frequency noise increase of partially blocked nanopores (5). For nanopores with resistance values that correspond to the nanopore geometry, we show that the low-frequency 1/*f* noise behaves according to Hooge's phenomenological relation. These nanopores exhibit a linear scaling of the noise power with the inverse number of charge carriers, as is observed in many condensed-matter systems (20). This behavior may also explain the unexpected scaling of the noise power with the inverse of the conductance found for biological pores (21). For our solid-state nanopores, we obtain a Hooge parameter of $\alpha = (1.1 \pm 0.1) \times 10^{-4}$.

The results obtained offer a good description of the noise in our solid-state nanopores over the whole frequency range. They not only enable us to improve on characteristics of partially blocked nanopores by addressing their surface properties (4, 22), but also provide means to design and optimize nanopore experiments where the translocation of DNA is probed. As an illustration, we have shown that DNA translocation events are even detectable for nanopores with diameters as large as 100 nm, provided that measurements are performed at low salt concentrations (≈1 mM KCl).

Materials and Methods

Single solid-state nanopores are fabricated in thin 20-nm low-stress SiN membranes. Most membranes were covered by 10–20 nm sputtered SiO_2 on each side. Formation of a nanopore results from the exposure of the membrane to a tightly focussed electron beam using a transmission electron microscope (TEM) (23). The resulting nanopores can be imaged directly in the TEM, as shown in Fig. 1*a Inset*. Details of the fabrication process are described in ref. 24. In our experiments, nanopores with diameters between 3.7 and 51.0 nm are used. Before use, the nanopores are either exposed to an oxygen flow at elevated temperatures (300, 600, or 900°C), flushed with ethanol, or subjected to an oxygen plasma. The pretreatment removes organic contaminants and enhances the hydrophilicity of the surface. The different pretreatments did not yield systematic differences for the nanopore resistance or noise. Nanopores were mounted in the setup using a microfluidic flow cell. Solutions are prepared by adding Milli-Q filtered water (Millipore) to a stock solution of 1 M KCl with 10 mM Tris·HCl buffer at pH = 7.5. Ionic currents are detected by Ag/AgCl electrodes, connected to an amplifier operating in resistive feedback mode (Axopatch 200B, Axon Instruments). The currents are low-pass filtered using an external 8-pole Bessel filter, with a cutoff frequency of 49.9 kHz. The signal is digitized at 250 or 500 kHz. Power spectra result from ≈2 s of current recordings using Labview (National Instruments). The data are smoothed by averaging over an increasing number of nearest neighbor points. All calculations presented are performed using a cylindrical nanopore, with a length of L_{pore} = 25 nm, and surface charge values from ref. 15. The values of the amplifier configuration are given by R_f = 500 MΩ, C_f = 1 pF, $i_a = 3.2 \times 10^{-30}$ A^2/Hz and $e_a = 9 \times 10^{-18}$ V^2/Hz. For the calculation of the current power spectral density of our nanopore sample, we use $e_a = 6 \times 10^{-16}$ V^2/Hz, a value that is relatively high compared to the expected performance of the amplifier. This is likely to be the result of an overestimation of the value of R_c. The *SNR* is calculated by using an applied voltage of 100 mV, and C_p = 30 pF with $D = 2.7 \times 10^{-1}$. Integration of the current power spectrum is performed from 0.5 Hz.

ACKNOWLEDGMENTS. We thank D. Krapf, M. Y. Wu, and K. Halma for contributions to the experimental work and S. Lemay for discussions. This work is part of the research programme of the "Stichting voor Fundamenteel Onderzoek der Materie (FOM)," which is financially supported by the "Nederlandse Organisatie voor Wetenschappelijk Onderzoek (NWO)."

1. Kasianowicz JJ, Brandin E, Branton D, Deamer DW (1996) Characterization of individual polynucleotide molecules using a membrane channel. *Proc Natl Acad Sci USA* 93:13770–13773.
2. Li J, *et al.* (2001) Ion-beam sculpting at nanometre length scales. *Nature* 412:166–169.
3. Dekker C (2007) Solid-state nanopores. *Nat Nanotechnol* 2:209–215.
4. Chen P, *et al.* (2004) Atomic layer deposition to fine-tune the surface properties and diameters of fabricated nanopores. *Nano Lett* 4:1333–1337.
5. Smeets RMM, *et al.* (2006) Nanobubbles in solid-state nanopores. *Phys Rev Lett* 97:088101.
6. Bezrukov SM, Kasianowicz JJ (1993) Current noise reveals protonation kinetics and number of ionizable sites in an open protein ion channel. *Phys Rev Lett* 70:2352–2355.
7. Nekolla S, Andersen C, Benz R (1994) Noise-analysis of ion current through the open and the sugar-induced closed state of the lamb channel of Escherichia-coli outer-membrane-evaluation of the sugar binding-kinetics to the channel interior. *Biophys J* 66:1388–1397.
8. Andersen C, Jordy M, Benz R (1995) Evaluation of the rate constants of sugar-transport through maltoporin (lamb) of Escherichia-coli from the sugar-induced current noise. *J Gen Physiol* 105:385–401.
9. Bezrukov SM, Kullman L, Winterhalter M (2000) Probing sugar translocation through maltoporin at the single channel level. *FEBS Lett* 476:224–228.
10. Kullman L, Winterhalter M, Bezrukov SM (2002) *Biophys J* 82:803–812.
11. Rostovtseva TK, Bezrukov SM (1998) ATP transport through a single mitochondrial channel, VDAC, studied by current fluctuation analysis. *Biophys J* 74:2365–2373.
12. Nestorovich EM, Danelon C, Winterhalter M, Bezrukov SM (2002) Designed to penetrate: Time-resolved interaction of single antibiotic molecules with bacterial pores. *Proc Natl Acad Sci USA* 99:9789–9794.
13. Bezrukov SM, Winterhalter M (2000) Examining noise sources at the single-molecule level: 1/f noise of an open maltoporin channel. *Phys Rev Lett* 85:202– 205.
14. Siwy Z, Fulinski (2002) A origin of 1/f(alpha) noise in membrane channel currents. *Phys Rev Lett* 89:158101.
15. Smeets RMM *et al.* (2006) Salt dependence of ion transport and DNA translocation through solid-state nanopores. *Nano Lett* 6:89–95.
16. Benndorf K (1995) Low-Noise Recording. in *Single-Channel Recording,* eds Sakmann B, Neher E (Kluwer Academic/Pelenum, New York), 2nd Ed, pp 129–145.
17. Sherman-Gold R (1993–2006) *The Axon CNS Guide to Electrophysiology and Biophysics Laboratory Techniques* (Molecular Devices, Sunnyvale, CA).
18. Westerlund S, Ekstam L (1994) Capacitor theory. *IEEE Transactions on Dielectrics and Electrical Insulation* 1:826–839.
19. Hooge FN (1969) 1/F noise is no surface effect. *Phys Lett* 29A:139.
20. Hooge FN, Kleinpenning TGM, Vandamme LKJ (1981) Experimental studies on 1/f noise. *Rep Prog Phys* 44:479–532.
21. Wohnsland F, Benz R (1997) 1/f-noise of open bacterial porin channels. *J Membr Biol* 158:77–85.
22. Wanunu M, Meller A (2007) Chemically modified solid-state nanopores. *Nano Lett* 7:1580–1585.
23. Storm AJ, *et al.* (2003) Fabrication of solid-state nanopores with single-nanometre precision. *Nat Mater* 2:537–540.
24. Krapf D, *et al.* (2006) Fabrication and characterization of nanopore-based electrodes with radii down to 2 nm. *Nano Lett* 6:105–109.